ORIGINAL RESEARCH ARTICLE

On the Inability of the Moving Interface Model to Predict Isothermal Solidification Time During Transient Liquid Phase (TLP) Bonding of Ni-Based Superalloys

MAJID POURANVARI, ALI GHASEMI, and ARMIN SALMASI

Understanding diffusion-induced isothermal solidification time during transient liquid phase bonding is vital in producing intermetallic-free robust joints. The isothermal solidification completion time is overestimated by the existing analytical models, even by the closest one to the real bonding conditions, known as the moving interface model. It was found that the boride formation in the diffusion affected zone of Ni-based superalloy upon using B-containing filler metals is one of the reasons behind the inability of the moving interface model to predict the isothermal solidification completion time accurately, which has received scant attention in the literature. Moreover, simplified assumptions in deriving the moving interface model such as constant interfacial solute concentration, which is only valid for binary systems, along with the independency of diffusion coefficient to concentration introduce errors when estimating the isothermal solidification time using the moving interface model. The significant discrepancy between the predicted and experimentally obtained isothermal solidification times reinforces the idea that the existing moving interface analytical model needs to be modified.

https://doi.org/10.1007/s11661-021-06497-x

I. INTRODUCTION

THE emergence of the transient liquid phase (TLP) bonding process as a novel joining technique with a solid/liquid (S/L) interface nature has introduced an unprecedented opportunity in many technological fields, including turbine industries, to join/repair Ni-based superalloys.[1–6] The easy assembly of the gas turbine engine segments with intricate geometries by an efficiency approaching 100 pct[7] can be considered as one of the revolutions in the turbine industry, which became feasible after the birth of the TLP bonding process. Based on the studies focused on the TLP bonding of solid solution (*e.g.*, Hastelloy X),[8–10] precipitate hardening (*e.g.*, IN738),[11–14] and single crystal[15–17] Ni-based superalloys as suitable candidates for turbine applications, it is fair to conclude that high-performance joints are achievable through this bonding process.

MAJID POURANVARI is with the Department of Materials Science and Engineering, Sharif University of Technology, 11365-9466, Tehran, Iran. Contact e-mail: pouranvari@sharif.edu ALI GHASEMI is with the Department of Mechanical Engineering, McMaster University, Hamilton, ON L8S 4L7, Canada. Contact e-mail: ghasemia@mcmaster.ca ARMIN SALMASI is with the Department of Materials Science and Engineering, KTH Royal Institute of Technology, 100 44 Stockholm, Sweden.

Manuscript submitted April 20, 2021; accepted October 8, 2021.
Article published online November 7, 2021

While sharing the same concept of bonding with the brazing process from the interfacial interaction viewpoint, the TLP bonding process benefits from an isothermal solidification stage, eliminating the formation of undesirable eutectic microconstituents perceptible in brazements with athermal solidification nature.[18–22] Furthermore, the accomplishment of the isothermal solidification stage during the TLP bonding process can mitigate the penalties associated with the low strength and low melting point of the typical brazed joints that originate from the brittleness of the eutectic phases formed during the cooling stage at temperatures lower than the bonding temperature (T_{Bonding}).[23] Given the fact that the reliability of the TLP bonded Ni-based superalloys during service is tied to the absence of these undesirable phases, the combination of bonding parameters should be adjusted with enough care to guarantee the completion of isothermal solidification during the bonding period.

Experimental methods are currently tackled by expensive trial and error through manipulating process parameters to end up with robust eutectic-free joints. Since this implies high experimental costs, predictive methods such as analytical models are essential to estimate the isothermal solidification completion time (t_{IS}) or to narrow down the testing time cycles even at the design stage. Despite the time and cost benefits of the analytical approaches, the existing models suffer

from insufficient accuracy in predicting the t_{IS} in Ni-based superalloys, especially when boron-containing filler metals (FMs) are employed. As discussed in the following sections, the closest analytical model to the real TLP bonding conditions (the moving interface model) significantly overestimates t_{IS}.

In this study, the moving interface analytical model has been implemented to predict the t_{IS} for different Ni-based superalloys when B-containing FMs are used. The analytical model overestimation roots were explored by considering the base material (BM) chemical composition, boron/BM interactions in the diffusion affected zone (DAZ) during the TLP bonding process, and simplified assumptions in deriving the moving interface analytical model and diffusion thermodynamic and diffusion kinetic parameters. The knowledge gained from comparing the analytical outcomes and the experimental results bolds the moving interface model's inability to predict t_{IS}. By scrutinizing the fundamentals behind isothermal solidification, proper solutions are proposed to deal with the prediction challenges efficiently and expand the general understanding of the TLP bonding process.

II. PREDICTION OF ISOTHERMAL SOLIDIFICATION TIME USING MOVING INTERFACE ANALYTICAL MODEL

A. *The Model*

The study of the TLP bonding process through an analytical approach has received some attention within the literature.[1,24–32] The outcomes are quite different depending on the solution method of Fick's diffusion equation, interface movement considerations, and the boundary and initial conditions.[24] To have a reliable analytical model consistent with the physics of the TLP bonding process, the followings need to be taken into account: (i) Migration of the solid/liquid interface,[33] (ii) Equilibrium conditions at the solid/liquid interface,[21] and (iii) Unsteady state diffusion of the MPD from a source with finite dimensions. The most accurate analytical model is the moving interface model proposed by Lesoult.[34] Figure 1 shows the Ni-B phase diagram (Figure 1(a)) and the corresponding boron concentration profile (Figure 1(b)) during isothermal solidification in Ni/Ni-B/Ni system. Based on the moving interface model (Figure 1), the solid/liquid interface location ($X(t)$) is a function of time. By assuming that $X(t) = K\sqrt{4Dt}$, and $X(\infty, t) = C_{BM}$, the t_{IS} can be calculated by Eq. [1]:[34]

$$t_{IS} = \frac{W_{max}^2}{16K^2D} \qquad [1]$$

in which W_{max}, and D denote the maximum gap size and the MPD diffusion coefficient in the solid phase, respectively. K is a constant which can be calculated by Eq. [2]:

$$\frac{K[1 - erf(K)]\sqrt{\pi}}{\exp(-K^2)} = \frac{C_{\gamma L} - C_{BM}}{C_{L\gamma} - C_{\gamma L}} \qquad [2]$$

In Eq. [2], $C_{\gamma L}$, $C_{L\gamma}$, and C_{BM} signify the MPD concentration of solid phase at the solid/liquid interface, MPD concentration of liquid phase at the solid/liquid interface, and the MPD concentration in the bulk of the BM, respectively. This model provides valuable information about the factors affecting isothermal solidification. The solid-state diffusivity or diffusion coefficient of MPD atoms into the BM (D) represents the role of diffusion kinetics. The MPD concentration difference between the solid phase at the solid/liquid interface and the BM, $(C_{\gamma L} - C_{BM})$, represents the contribution of diffusion thermodynamics or the driving force behind the diffusing atoms on the t_{IS}. Moreover, the concentration difference between the equilibrium chemical composition of the liquid phase and solid phase, $(C_{L\gamma} - C_{\gamma L})$, along with the maximum liquid width (W_{max}) after the dissolution stage, highlights the influence of the number of diffusing substances on the t_{IS}.[21]

B. *Solid-State Diffusion Data*

To be able to implement Eq. [1] for the prediction of t_{IS}, the solid-state diffusivity of the MPD atom in the BM (D) in tandem with the thermodynamic data at $T_{Bonding}$ should be known.[25–27] Unfortunately, there is limited information on the diffusivity of MPDs (*i.e.*, B) in the Ni-based superalloys. Therefore, finding the experimental diffusivity data before using Eq. [1] seems to be essential for materials with unknown diffusion kinetics and thermodynamics.

To resolve the abovementioned issue, Ikawa *et al.*[30] proposed an analytical-experimental approach to finding out the diffusion data. By calculating the atomic flux of MPD and consequently the amount of diffusing atoms from the liquid phase into the solid phase in a moving interface scenario, the width of isothermally solidified zone (X) in a half-joint can be predicted as a function of time (t):

$$X = \left[\left(\frac{C_{\gamma L} - C_{BM}}{C_{L\gamma} - C_{\gamma L}}\right)\frac{2\exp(-K^2)\sqrt{D}}{(1 - erf(K))\sqrt{\pi}}\right]\sqrt{t} \qquad [3]$$

In Ni-based superalloys bonded by B-containing FMs, the magnitude of K is small enough to be assumed as zero.[24] By substituting $K = 0$ in the above equation, it can be simplified as follows:

$$X = \frac{2}{\sqrt{\pi}}\left(\frac{C_{\gamma L} - C_{BM}}{C_{L\gamma} - C_{\gamma L}}\sqrt{D}\right)\sqrt{t} \qquad [4]$$

In Eq. [4], the width of ISZ in the half-joint can be converted to the width of the remaining liquid phase using the following equation:

$$\frac{W_{max}}{2} - \frac{X_{ASZ}}{2} = \frac{2}{\sqrt{\pi}}\left(\frac{C_{\gamma L} - C_{BM}}{C_{L\gamma} - C_{\gamma L}}\sqrt{D}\right)\sqrt{t} \qquad [5]$$

in which $\frac{X_{ASZ}}{2}$ denotes the width of the remaining liquid phase at $T_{Bonding}$, which could not find the chance to

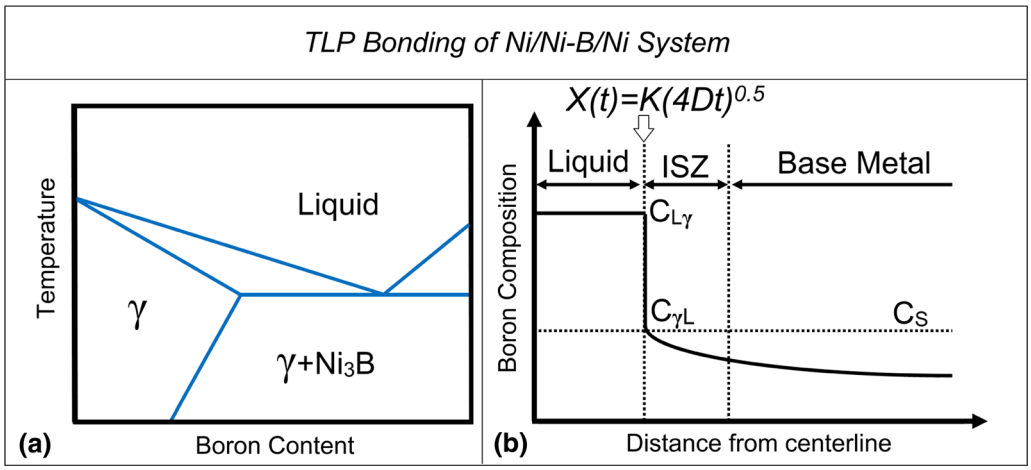

Fig. 1—(*a*) Schematic of the Ni-B phase diagram and (*b*) the corresponding boron concentration during isothermal solidification of Ni/Ni-B/Ni bonding system. The boron content of the BM does not exceed the solid solubility of boron in the base metal. Therefore, conventional standard TLP models predict a boride-free substrate.

experience isothermal solidification, but athermal solidification. Equation [5] suggests that there is a linear correlation between X_{ASZ} and $\sqrt{t}$ with a slope of $m = -\frac{4}{\sqrt{\pi}}\left(\frac{C_{\gamma L}-C_{BM}}{C_{L\gamma}-C_{\gamma L}}\right)\sqrt{D}$. For a given $T_{Bonding}$, the value of m is obtained by performing the TLP bonding process at different holding times and measuring the width of the athermal solidification zone at each period.[27] By using the following Arrhenius equation, D can be linked to the temperature[35]:

$$D = D_0 \exp\left(\frac{-Q}{RT}\right) \quad [6]$$

in which D_0 and Q denote the diffusion constant (frequency factor of diffusion) and activation energy for MPD diffusion in the solid phase. R and T are the gas constant and bonding temperature ($T_{Bonding}$), respectively. Equation [6] can be used to rewritten m as follows:

$$m = -\frac{4}{\sqrt{\pi}}\left(\frac{C_{\gamma L}-C_{BM}}{C_{L\gamma}-C_{\gamma L}}\right)\sqrt{D_0 \exp\left(\frac{-Q}{RT}\right)} \quad [7]$$

After taking the logarithm of both sides:

$$Ln(-m) = A - \frac{Q}{2RT} \quad [8]$$

where $A = \mathrm{Ln}\left[\frac{4}{\sqrt{\pi}}\left(\frac{C_{\gamma L}-C_{BM}}{C_{L\gamma}-C_{\gamma L}}\right)\right] + \frac{1}{2}\mathrm{Ln}(D_0)$. By performing the TLP bonding process at different $T_{Bonding}$ and plotting $Ln(-m)$ as a function of $\frac{1}{T}$, the Q and D_0 can be determined from the slop and Y-axis intercept of the plotted line, respectively. Afterwards, Eqs. [6] and [1] can be employed to calculate the D and t_{IS}, respectively, at any desired $T_{Bonding}$. The data related to the thermodynamics of diffusion such as $C_{L\gamma}$, $C_{\gamma L}$, and C_{BM} should also be known to predict the t_{IS} using Eq. [1].

To put this into conclusion, the following steps need to be taken before being able to implement the moving interface analytical model for prediction of t_{IS}: (1) determining the slope (m) of the linear plot correlating X_{ASZ} to $\sqrt{t}$ at different $T_{Bonding}$, (2) obtaining the slope and Y-axis intercept of the linear plot correlating $\mathrm{Ln}(-m)$ to $\frac{1}{T}$ to calculate the Q and D_0, respectively, (3) using Eq. [6] to calculate the diffusion coefficient of MPD in the solid phase at the desired temperature, and (4) using Eq. [1] to predict the t_{IS}.

III. ASSESSMENT OF THE MOVING INTERFACE MODEL

In this section, the validity of the moving interface model to predict t_{IS} during TLP bonding of Ni-base superalloys is assessed by comparing the experimental data available in the literature[26–28,36–38] with the predicted results (Table I).

Table I gives the bonding temperature ($T_{Bonding}$), the initial thickness of the FM, composition of the FM, maximum liquid wide (W_{max}), the thermodynamic values, the kinetics data, the experimentally determined and the predicted t_{IS} for each superalloy. For the sake of consistency, the calculations were redone based on the results provided in the cited references to estimate the t_{IS} based on the moving interface model prediction using the procedure explained in Section II. The following points should be mentioned regarding the data presented in Table I:

1. *Maximum liquid width* (W_{max}) The W_{max}, that plays a significant role in determining the t_{IS}, is dictated by the complex interaction of liquid FM and solid BM at the bonding temperature. Here, the W_{max} was determined using micrographs provided in the references corresponding to each TLP bonded system.
2. *Thermodynamic data* The $C_{L\gamma}$ and $C_{\gamma L}$ values are controlled by the equilibrium between solid and liquid at the bonding temperature. The diffusion thermodynamic data were calculated for a simplified Ni-B binary system and multi-component FMs using Thermo-Calc Software. Therefore, two

different approaches are used to determine the $C_{L\gamma}$ and $C_{\gamma L}$:

Binary Ni-B phase diagram In this case, the BM, a Ni-based superalloy, was assumed to be pure Ni, and the multi-component FMs were simplified to a Ni-B binary FM in which B is the only MPD element. Considering the fact that the Ni element is the basis of Ni-based superalloys and the S/L interface velocity is controlled by the diffusion of the fastest MPD element, which is B in the case of B-containing FMs,[29] the former and latter assumptions are justifiable. The binary phase diagram of Ni-B calculated by Thermo-Calc Software Version 2021a[39] is shown in Figure 2.

B-excluded FM vs. B Isopleths In this case, it is assumed that the dissolution of the BM during the TLP bonding process is not happening and the first layer of the liquid phase isothermally solidified on the BM has the same chemical composition as that of the B-excluded FM (the B concentration is zero in the solidified layer). The purpose is to find the equilibrium B concentration between the liquid FM and the defined solid layer during the TLP bonding process. For example, For BNi-9 FM, it is assumed that the liquid phase has the initial chemical composition of Ni–14.78Cr–16.97B (at. pct), and the first layer of the isothermally solidified liquid at the interface has the chemical composition of Ni–14.78Cr (at. pct). In the calculated isopleth, the chemical composition of the left-hand side endmember is fixed at B-excluded FM chemical composition, and it is assumed that Ni is a dependent variable. The X-axis of the isopleth is the atomic percent of B. The B element is substituted by the Ni in the calculated isopleths. For instance, in the calculated isopleth for BNi-9, the chemical composition of the left-hand side endmember is fixed at Ni–14.78Cr (at. pct), and B is substituted by Ni. At a specific temperature (*i.e.*, bonding temperature) in the isopleths, the $C_{\gamma L}$ and $C_{L\gamma}$ can be obtained. The isopleths for the different FMs listed in Table 1 calculated by Thermo-Calc Software Version 2021a[39] are shown in Figure 3. In the calculated metastable isopleth for BNi-2 and BNi-9, as well as the calculated equilibrium isopleth for BNi-3 FM, the solidus and liquidus temperatures were found to be slightly higher than their corresponding experimental values (up to ~ 50 °C). The same level of discrepancy has been reported between the experimental and Thermo-Calc calculation results for D-15, BNi-2 and Ni-Si-B systems.[40–42] Therefore, in some cases, the bonding temperature was lower than the predicted solidus temperature by the provided isopleths. In these cases, the minimum temperature at which the liquid and solid phases exist at equilibrium conditions was used instead to obtain thermodynamic data ($C_{\gamma L}$ and $C_{L\gamma}$). The minimum temperatures at which solid and liquid phases co-exist were found to be 1080 °C, 1125 °C, and 1105 °C for BNi-2, BNi-9 and BNi-3, respectively. It is of note that in contrast to binary systems, $C_{\gamma L}$ and $C_{L\gamma}$ are not fixed during the isothermal solidification in multi-component systems.[39] Nevertheless, these values were assumed to be constant even in this case since the moving interface model does not account for the change in the concentration of equilibrium solid and liquid phases at the interface.

3. *Diffusion data* The boron diffusivity into the superalloy is a key factor that controls the kinetics of diffusion and hence t_{IS}. The activation energy (Q) and diffusion frequency factor (D_0) for B diffusion were determined using the same procedure explained in section II–B (Eqs. [3] to [8]). It is of note that the thermodynamic values should be known for calculating D_0. Since the thermodynamic parameters are a function of temperature, the reported D_0 in Table I is the average of values obtained at each temperature. It should also be noted that the diffusion coefficient is concentration-dependent, which can affect the prediction of a moving interface model.

The outcomes of the t_{IS} calculated by Eq. [1] in the current study, as well as the t_{IS} obtained by the experimental approach in References 26–28,36–38, are summarized in Table I. According to Table I, the t_{IS} values obtained by the moving interface model are noticeably larger than that of the experimentally determined isothermal solidification times. The reasons are discussed in the following section.

IV. ISOTHERMAL SOLIDIFICATION ACCELERATED BY *IN SITU* BORIDE PRECIPITATION

The isothermal solidification rate during TLP bonding of Ni-based superalloys using B-containing filler metals is controlled by the B flux into the BM, which is governed by the diffusion kinetics (B diffusivity into the BM) and diffusion thermodynamics (*i.e.* solid solubility of B into the BM). Table I shows that the time required for isothermal solidification in real multi-component systems are shorter than values predicted by the moving interface model. Therefore, a mechanism for the acceleration of isothermal solidification should exist. Several possibilities need to be considered:

1. *Squeezing out of the liquid phase from the joint gap* This factor has been accounted for the difference observed between the calculated and the experimentally determined t_{IS} in Reference 44. The liquid extrusion can reduce the liquid phase volume present in the joint gap and shorten the isothermal solidification time. However, the role of this factor

Table I. Diffusion Kinetic and Thermodynamic Data Along With the Experimental Bonding Variables Used in the Literature to Compare the Isothermal Solidification Time (t_{IS}) Predicted by the Moving Interface Model to That of Obtained Experimentally

					Diffusion Kinetic and Thermodynamic Data Based on the Binary Ni-B Phase Diagram				
Material	FM_{Comp}	$T_{Bonding}$	C_{BM}	Q	D_0	D	$C_{\gamma L}$[c]	$C_{L\gamma}$[c]	K
IN718[27]	BNi-2	1000	0.037	165	0.002082	3.53×10^{-10}	0.264[d]	15.98[d]	0.008225
		1050				6.36×10^{-10}	0.264[d]	15.98[d]	0.008225
		1100				1.10×10^{-9}	0.263	15.71	0.008332
IN738[26]	BNi-9	1100	0.06	218	0.098644	5.01×10^{-10}	0.263	15.71	0.007477
		1150				9.81×10^{-10}	0.259	14.27	0.008087
Mar-M247[36]	Ni–5.18Cr–4.32Co–2.15W–0.55Ta-17B (at. pct)	1150	0.08	199[a][25]	0.019498	9.66×10^{-10}	0.259	14.27	0.007267
IN600[37]	BNi-9	1080	0	209[25]	0.009489	8.09×10^{-11}	0.264[4]	15.98[d]	0.00958
Pure Ni[28,38]	BNi-3	1065	0	226[b][25]	0.034302	5.15×10^{-11}	0.264[4]	15.98[d]	0.00958
		1075				5.99×10^{-11}			0.00958
Units	—	°C	at. pct B	kJ/mol	m^2/s	m^2/s	at. pct B	at. pct B	—

	Diffusion Thermodynamic Parameters Based on the FM Isopleths									
Material	Q	D_0	D	$C_{\gamma L}$[e]	$C_{L\gamma}$[e]	K	W_{max}	t_{IS} Exp.	t_{IS} Anal. Based on Binary Ni-B	t_{IS} Anal. Based on FM Isopleths
IN718[27]	165	0.00312	5.29×10^{-10}	0.201	14.33	0.006598	54	60	127	132
			9.54×10^{-10}	0.201	14.33	0.006598	60	40	87	90
			1.65×10^{-9}	0.202	13.53	0.00704	66	20	59	56
IN738[26]	218	0.145827	7.41×10^{-10}	0.216	14.52	0.006196	130	> 420 < 480	628	619
			1.45×10^{-9}	0.212	13.72	0.006394	155	> 240 < 300	390	422
Mar-M247[36]	199[a][25]	0.039185	1.94×10^{-9}	0.207	14.29	0.005117	115	240	270	271
IN600[37]	209[25]	0.012877	1.10×10^{-10}	0.216	14.52	0.008602	60	240	505	461
Pure Ni[28,38]	226[2][25]	0.020464	3.07×10^{-11}	0.284	13.68	0.012125	27	120	161	168
			3.57×10^{-11}			0.012125	71	360	955	999
Units	kJ/mol	m^2/s	m^2/s	at. pct B	at. pct B	—	μm	min	min	min

The diffusion thermodynamic data were determined from both Ni-B binary phase diagram and B-excluded FM *vs.* B concentration isopleths provided in Figs. 2 and 3.

[a]The reported Q value for Mar-M247 was calculated for Mar-M247/BNi-9/Mar-M247 system in Ref. 25. The same Q was used for the TLP bonded Mar-M247 using Ni-5.18Cr-4.32Co-2.15W-0.55Ta-17B (at. pct) since it is also a B-containing FM.

[b]The reported Q value for pure Ni was calculated for Ni/Ni-1.23Co-21.71B(at pct)/Ni system in Ref. [25]. The same Q was used for the TLP bonded pure Ni using BNi-3 since it is also a B-containing FM.

[c]The thermodynamic data ($C_{\gamma L}$ and $C_{L\gamma}$) were calculated by Thermo-Calc Software-TC Binary Solutions V1.1 Database.

[d]In the binary Ni-B phase diagram, liquid, and solid phases exist at equilibrium conditions at temperatures higher than 1093 °C. Therefore, when the bonding temperature was lower than 1093°C, thermodynamic data ($C_{\gamma L}$ and $C_{L\gamma}$) of this temperature were used instead.

[e]The thermodynamic data ($C_{\gamma L}$ and $C_{L\gamma}$) were calculated by Thermo-Calc Software- TCNI /NI alloys database version 10.[43]

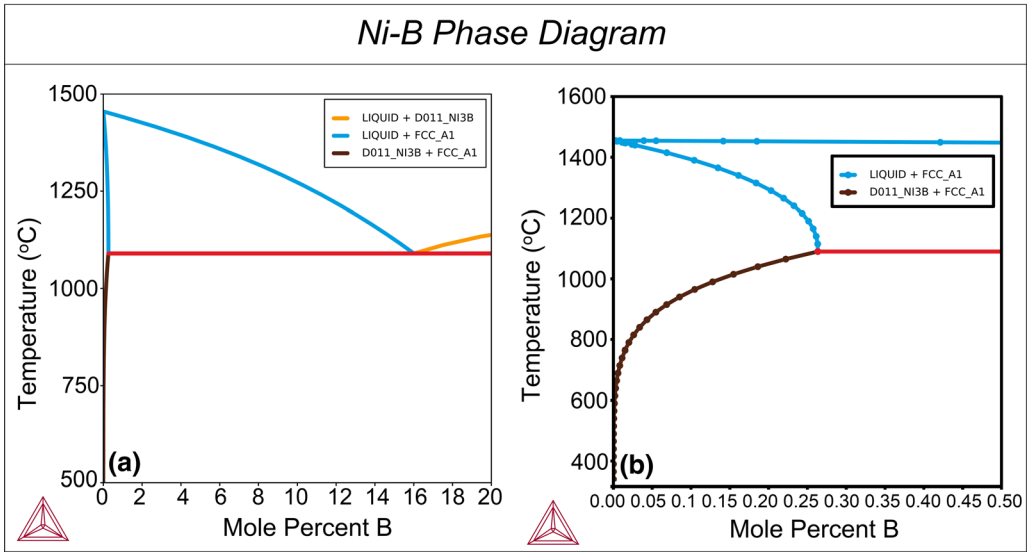

Fig. 2—Ni-B equilibrium binary phase diagram calculated by Thermo-Calc Software-TC Binary Solutions V1.1 Database for an atomic B concentration range of (*a*) 0 to 20 at. pct, and (*b*) 0 to 0.5 at. pct. $C_{\gamma L}$ and $C_{L\gamma}$ values used in the moving interface model were determined from (a) and (b), respectively.

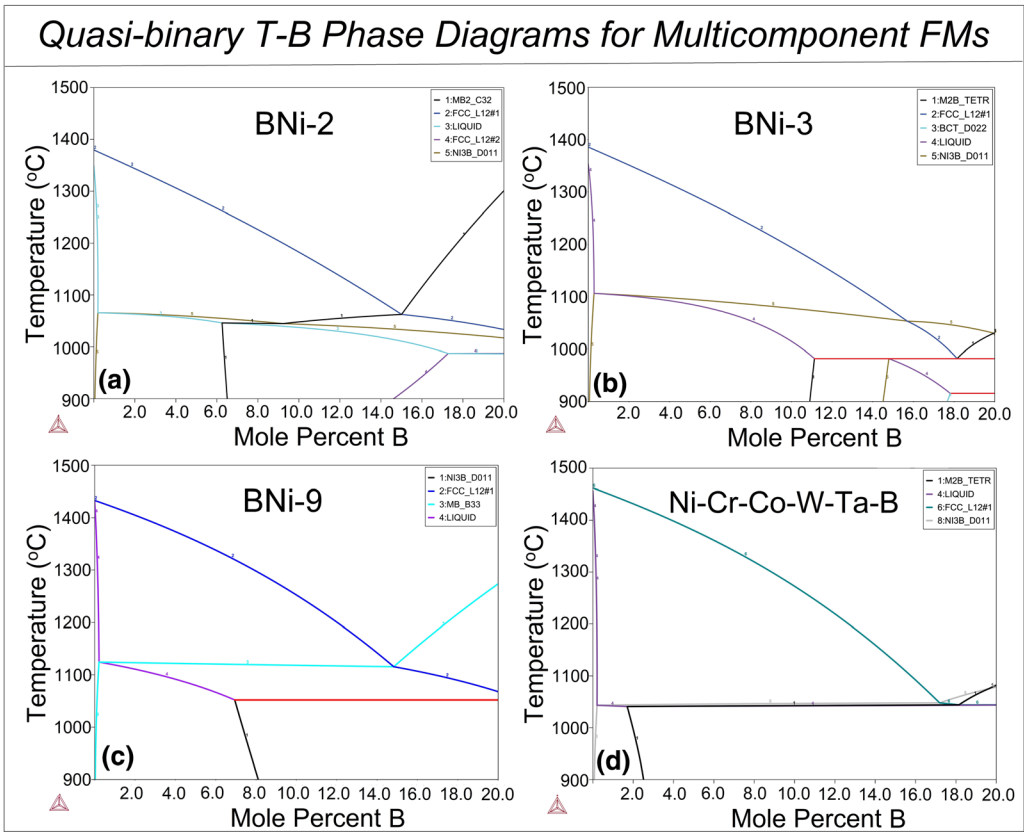

Fig. 3—The calculated isopleths for (*a*) BNi-2, (*b*) BNi-3, (*c*) BNi-9, and (*d*) Ni–5.18Cr–4.32Co–2.15W–0.55Ta–17B (at. pct) FMs using Thermo-Calc Software-TCNI/Ni-alloys database version 10.[43] The chemical composition of the left-hand side endmember is fixed at B-excluded FM chemical composition, and it is assumed that Ni is a dependent variable. The *X*-axis of the isopleth is the atomic percent of B. The B element is substituted by the Ni in the calculated isopleths. It should be noted that (a) and (c) are metastable isopleths while (b) and (d) are equilibrium isopleths.

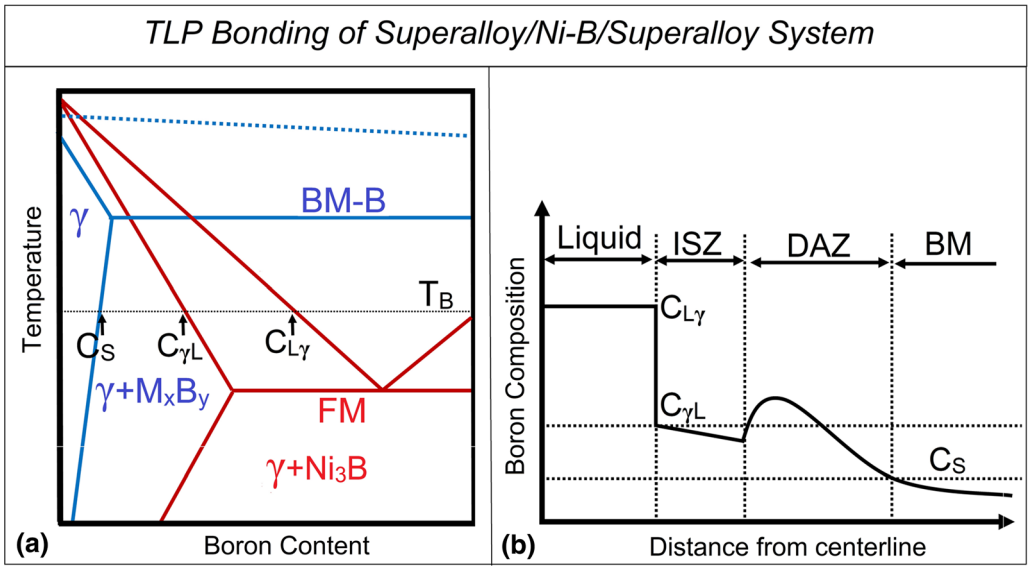

Fig. 4—TLP bonding in a real multi-component system: (*a*) schematic of the quasi-binary T-B phase diagram for BM (multi-component superalloy)/B and schematic binary phase diagram of Ni-B (filler metal). (*b*) B concentration profile during isothermal solidification of Superalloy/Ni-B/Superalloy bonding system. The solid solubility of B at the S/L interface is $C_{\gamma L,}$ which is higher than the solid solubility of B in the BM (C_S). Therefore, the boron content of the BM can exceed the solid solubility of boron in the BM resulting in *in situ* boride precipitation in the diffusion affected zone (DAZ) if the bonding temperature (TB) is below the boride solvus temperature of the BM.

is ruled out in the analysis presented in this work because the W_{max} was measured using real micrographs.

2. *The role of grain boundaries* The grain boundaries (GBs) can also affect the kinetics of diffusion, which can contribute to the MPD mass transport flux into the base superalloy. However, the contribution of the grain boundary diffusion at a temperature higher than 0.75 T_m (where T_m is the equilibrium melting temperature in K) is less pronounced.[45] Therefore, considering the fact that bonding temperature during diffusion brazing of Ni-base superalloys is typically higher than 0.75 T_m, the grain size of the base metal is not a key factor in determining the isothermal solidification rate. Moreover, GB liquation and liquid penetration at grain boundaries accelerate the isothermal solidification process by increasing the effective solid-liquid interfacial area and increasing the rate of solute diffusion into the BM.[46] However, this phenomenon was not reported in any of the cases studied in this work. Liquation during TLP bonding occurs when the bonding temperature is higher than the eutectic temperature of the superalloy/boron system.[21,38,47] It is of note that all GB phenomena are less pronounced in large-grained BMs. For instance, some superalloys given in Table I are in as-cast condition (*i.e.*, IN718, IN738, Mar-M247) with coarse-grained structure. Therefore, the GB phenomena do not play a key role in accelerating the kinetics of isothermal solidification in these cases. Nevertheless, considering the "apparent diffusion coefficient" concept, all these factors are embedded in the calculated diffusivity of B into the BM. In other words, the D values used in this study have been determined using an experimental approach at real bonding conditions, where the B atoms of a multi-component FM diffuse into a multi-component Ni-based superalloy. Therefore, the D values used are "apparent D" values that measure the real mass transport of B into the BM during the TLP bonding process.

3. *Composition dependence of the B diffusivity* Generally, the diffusion coefficient varies with composition. For example, it is reported that the diffusion coefficient for carbon in FCC-Fe at 1000 °C is 2.5×10^{-11} m^2 s^{-1} at 0.15 wt pct C, but it rises to 7.7×10^{-11} m^2 s^{-1} in solutions containing 1.4 wt pct C due to lattice strain induced by the C atoms.[45] In the case of TLP bonding, the composition of the BM is evolved during the progress of isothermal solidification by entering B atoms into the BM. This can modify the diffusivity of B during the progress of the isothermal solidification. However, there is no data in the literature regarding the composition dependency of B diffusion in Ni alloys.

4. *In situ boride precipitation* Generally, the TLP bonding of real multi-component systems is accompanied by precipitation of the boride phase in a region adjacent to the joint interface, called diffusion affected zone (DAZ). The *in situ* formation of boride precipitates can affect the boron's diffusion flux into the substrate during isothermal solidification.[40,48,49] However, the standard TLP models based on the Ni/Ni-B/Ni system does not predict the boride precipitation in the DAZ. This can be explained as follows:

   Boride precipitation in Ni/Ni-B/Ni system: At the bonding temperature, the liquid and solid phases are not at equilibrium conditions at the S/L

interface. Equilibrium conditions will be established at the S/L interface due to the FM/BM interdiffusion in the dissolution stage. After completion of the dissolution stage, the composition of the solid phase at the solid/liquid interface is $C_{\gamma L}$ which remains constant during the isothermal solidification stage (Figure 1(b)). The $C_{\gamma L}$ controls the amount of B diffusing into the BM. In the Ni/Ni-B/Ni system, the equilibrium B solubility at the interface $\left(C_{\gamma L}\right)$ is exactly the same as the B solubility in the bulk of the BM (C_S). Since the B concentration in the bulk of the pure Ni (BM) remains below $C_{\gamma L}\left(C<C_{\gamma L}=C_S\right)$ during the isothermal solidification, no boride precipitation takes place in this stage (see Figure 1(b)). However, boride precipitation has been reported during TLP bonding of pure Ni when the bonding temperature is less than the Ni-B eutectic temperature (*i.e.*, bonding using a FM with liquidus temperature less than the Ni-B eutectic temperature[38]). Gale and Wallace[47] proposed that diffusion of B from the liquid FM towards the BM before termination of the dissolution stage (*i.e.*, before achieving equilibrium at S/L interface) results in the formation of a binary Ni-B alloy in the substrate, which in turn leads to *in situ* boride precipitation in the substrate at the bonding temperature. They provided evidence that these boride precipitates are not formed during cooling but at the bonding temperature.

Boride precipitation in real multi-component systems It is of note that the presence of alloying elements, especially boride forming elements (*e.g.*, Cr, Mo, W, Ta, and Nb) in the real multi-component nickel-based superalloys, can affect the solubility of the B in the BM.[40] Figure 4 schematically shows the B concentration profile during isothermal solidification for a real multi-component system (superalloy/Ni-B/superalloy). The presence of boride forming elements in the BM can significantly reduce the solubility of B in the BM. Due to the lack of significant boride forming elements in the FM, the solid solubility of B at the S/L interface is higher than the solid solubility of B in multi-component nickel-based superalloys (*i.e.*, $C_{\gamma L} \succ C_S$). Therefore, in situ precipitation of the boride phase is possible in the multi-component systems if the bonding temperature is below the boride solvus temperature of the BM. It is well established that the diffusion of the B atoms into Ni-based superalloys during the liquid phase disappearance is accompanied by the formation of borides within the DAZ.[38,50–53]

In the absence of boride precipitation, as the isothermal solidification progresses, the concentration gradient of B atoms between the interface and the bulk of the BM decreases due to the increase of the B concentration in the BM bulk. This reduces the B diffusion flux and hence decelerates the isothermal solidification rate. However, in real multi-component superalloy/B-containing FM systems, the *in situ* boride precipitation during isothermal solidification can affect the diffusion flux of boron into the substrate during bonding. The reason behind such an observation is that the boride precipitation in real TLP bonding conditions leads to the consumption of the B atoms in the BM and the formation of B-free regions in the immediate vicinity of the precipitates. Therefore, a virtually constant and considerably high driving force of diffusion is applied to B atoms to diffuse in the BM during isothermal solidification. This significant driving force originates from the steep concentration gradient $(C_{\gamma L} - C_{BM})$ caused by the formation of B-free regions after boride precipitation in the DAZ.[19] Therefore, lack of the consideration of the boride formation in the DAZ in the conventional moving interface model leads to a decreased concentration gradient as the isothermal solidification progresses. Moreover, it has been proved that the B element can diffuse to the BM immediately after melting of the FM and prior to reaching T_{Bonding}, known as initial boron uptake.[32,54–56] The formation of borides in the DAZ in this period can consume a fraction of B elements in the liquid phase and leave behind a lower amount of B to diffuse in the BM during the isothermal solidification stage, which in turn reduces the t_{IS}. The difference between the predicted and experimental t_{IS} for IN718 and IN738 shows a descending trend by increasing the T_{Bonding}. This can be attributed to the reduced tendency of boride precipitation at higher T_{Bonding} due to the higher B solubility in the Ni-based superalloy. It has been shown that increasing the bonding temperature reduces the volume fraction of the boride phase in DAZ.[57,58] Therefore, the contribution of boride formation to the isothermal solidification rate is reduced at higher bonding temperatures.

Since the intermetallic phases such as borides typically exhibited low diffusion coefficient,[59] it is expected that effective diffusivity through γ-matrix + boride is expected to be reduced. However, considering the low volume fraction of the boride phases in DAZ (typically less than pctvol. 50), this factor is not expected to play a dominant role in the diffusion behavior of the MPD.[40,48] Nevertheless, the effect of *in situ* boride formation is considered in the kinetics of diffusion *via* the "apparent diffusion coefficient "concept used in this work. Therefore, the boride precipitation is only ignored in the parameters considering the diffusion thermodynamics in the moving interface model.

The abovementioned discussion supports the conclusion that although the moving interface analytical model can simulate the S/L interface migration, it is still only a diffusion-based model which fails to consider the B/BM reactions in the DAZ of the Ni-based superalloys during the TLP bonding process. The comparison of the analytical and experimental t_{IS} gives evidence that the B/BM reactions should be implemented in the analytical diffusion models to end up with reliable predictions. It is also worth noting that the thermodynamic parameters obtained from Ni-B binary phase diagram or the multi-component isopleths are assumed to be constant during the TLP bonding process and not a function of the time and/or concentration of diffusing element. It is shown by Sinclair[29,59] that during TLP bonding in a

two-phase ternary system (*e.g.* bonding a pure metal using an interlayer containing two solute), there is a continuous change in the composition of the remaining liquid, which is accompanied by continuous change in the corresponding MPD solubility in the solid. This issue cannot be captured using analytical models. Therefore, the thermodynamic parameters used in the analytical models cannot fully resemble the real TLP bonding condition. It means that the discrepancy observed between the analytical and experimental t_{IS} values is not merely attributable to the ignorance of boride formation but also the application of thermodynamic data from the binary Ni-B phase diagram or multi-component FM isopleths rather than real solid/liquid interface during the TLP bonding process. Moreover, the diffusion kinetic data are not assumed to be concentration-dependent, causing errors in the calculation of t_{IS}. On this account, the contribution of boride precipitation in the real systems on the errors associated with the isothermal solidification time calculations cannot be accurately and confidently identified due to presence of other sources of errors. One possible approach to find out what fraction of total errors is produced by the ignorance of boride precipitation is the utilization of a numerical approach in the future in which the effect of boride precipitation on the boron flux, dependence of diffusion coefficient on concentration and change in the B concentration in the liquid and solid phases at interface with time during the isothermal solidification stage are taken into account.

V. CONCLUSION

In summary, the kinetics of isothermal solidification during TLP bonding is not only determined by diffusivity of B and solid solubility of MPD at solid/liquid interface but also the in situ boride precipitation in the diffusion affected zone (DAZ). The significant errors between the experimental results and moving interface analytical model outcomes suggest the considerable role of *in situ* boride precipitation on isothermal solidification time during TLP bonding of nickel-based superalloys when B-containing filler metals are used. Therefore, to fulfil the existing vacancies and take another step toward finding a more accurate solution to predict the t_{IS}, in situ precipitation of the boride phases should be taken into account in developing an analytical solution. Moreover, to fully resemble the real conditions during the TLP bonding of multi-component systems, the thermodynamic parameters should be time and concertation-dependent in future models.

ACKNOWLEDGMENTS

The author would like to thank the anonymous reviewers for their helpful and constructive comments that significantly contributed to improving the final version of the paper. This research was supported by Iran National Science Foundation (INSF) under Grant No. 96006047. The contribution of Armin Salmasi was partly funded by the Swedish Foundation for Strategic Research (SSF), Contract RMA15-0062.

REFERENCES

1. W.D. MacDonald and T.W. Eagar: *Annu. Rev. Mater. Sci.*, 1992, vol. 22, pp. 23–46.
2. D.S. Duvall, W.A. Owczarski, and D.F. Paulonis: *Weld. J. (NY)*, 1974, vol. 53, pp. 203–14.
3. A. Ghasemi and M. Pouranvari: *Mater. Design*, 2019, vol. 182, p. 108008.
4. M. Pouranvari, A. Ekrami, and A.H. Kokabi: *J. Alloy. Compd.*, 2008, vol. 461, pp. 641–47.
5. O.A. Idowu, N.L. Richards, and M.C. Chaturvedi: *Mater. Sci. Eng. A*, 2005, vol. 397, pp. 98–112.
6. W.F. Gale and D.A. Butts: *Sci. Technol. Weld. Joining*, 2004, vol. 9, pp. 283–300.
7. D. F. Paulonis, D. S. Duvall and W. A. Owczarski, (Google Patents: 1972).
8. A. Ghasemi and M. Pouranvari: *Sci. Technol. Weld. Joining*, 2018, vol. 23, pp. 441–48.
9. A. Ghasemi and M. Pouranvari: *Sci. Technol. Weld. Joining*, 2019, vol. 24, pp. 342–51.
10. M. Kapoor, Ö.N. Doğan, C.S. Carney, R.V. Saranam, P. McNeff, and B.K. Paul: *Metall. Mater. Trans. A*, 2017, vol. 48A, pp. 3343–56.
11. N.P. Wikstrom, O.A. Ojo, and M.C. Chaturvedi: *Mater. Sci. Eng. A*, 2006, vol. 417, pp. 299–306.
12. O.A. Idowu, O.A. Ojo, and M.C. Chaturvedi: *Metall. Mater. Trans. A*, 2006, vol. 37A, pp. 2787–96.
13. M. Pouranvari, A. Ekrami, and A.H. Kokabi: *Sci. Technol. Weld. Joining*, 2014, vol. 19, pp. 105–10.
14. O.J. Adebajo and O.A. Ojo: *Metall. Mater. Trans. A.*, 2017, vol. 48A, pp. 26–33.
15. J.-D. Liu, T. Jin, N.-R. Zhao, Z.-H. Wang, X.-F. Sun, H.-R. Guan, and Z.-Q. Hu: *Sci. Technol. Weld. Joining*, 2010, vol. 15, pp. 194–98.
16. B. Riggs, B. Alexandrov, A. Benatar, and R. Xu: *Sci. Technol. Weld. Joining*, 2017, vol. 22, pp. 227–35.
17. X.B. Hu, N.C. Sheng, Y.M. Zhu, J.F. Nie, J.D. Liu, X.F. Sun, and X.L. Ma: *Metall. Mater. Trans. A*, 2020, vol. 51A, pp. 1689–98.
18. M. Pouranvari, A. Ekrami, and A.H. Kokabi: *J. Alloy. Compd.*, 2017, vol. 723, pp. 84–91.
19. M. Hosseini, A. Ghasemi, and M. Pouranvari: *Metall. Mater. Trans. A*, 2020, vol. 51A, pp. 5715–24.
20. M.M. Abdelfatah and O.A. Ojo: *Metall. Mater. Trans. A*, 2009, vol. 40A, pp. 377–85.
21. A. Ghasemi and M. Pouranvari: *Metall. Mater. Trans. A*, 2019, vol. 50A, pp. 2235–45.
22. A.G. Bigvand and O.A. Ojo: *Metall. Mater. Trans. A*, 2014, vol. 45A, pp. 1670–74.
23. S. Hadibeyk, B. Beidokhti, and S.A. Sajjadi: *J. Alloy. Compd.*, 2018, vol. 731, pp. 929–35.
24. Y. Zhou, W.F. Gale, and T.H. North: *Int. Mater. Rev.*, 1995, vol. 40, pp. 181–96.
25. Y. Nakao, K. Nishimoto, K. Shinozaki, and C. Kang: *Trans. Jpn. Welding Soc.*, 1989, vol. 20, pp. 60–65.
26. O.A. Ojo, N.L. Richards, and M.C. Chaturvedi: *Sci. Technol. Weld. Joining*, 2004, vol. 9, pp. 532–40.
27. M. Pouranvari, A. Ekrami, and A.H. Kokabi: *Can. Metall. Q.*, 2014, vol. 53, pp. 38–46.
28. W.F. Gale and E.R. Wallach: *Mater. Sci. Technol.*, 1991, vol. 7, pp. 1143–48.
29. C.W. Sinclair, G.R. Purdy, and J.E. Morral: *Metall. Mater. Trans. A*, 2000, vol. 31A, pp. 1187–92.
30. H. Ikawa, Y. Nakao, and T. Isai: *Trans. Jpn. Welding Soc.*, 1979, vol. 10, pp. 24–29.
31. T.C. Illingworth, I.O. Golosnoy, and T.W. Clyne: *Mater. Sci. Eng. A*, 2007, vol. 445, pp. 493–500.
32. E.D. Moreau and S.F. Corbin: *Metall. Mater. Trans. A*, 2020, vol. 18, pp. 1–11.

33. A. Ghanbar, D.E. Michael, and O.A. Ojo: *Philos. Magn.*, 2019, vol. 99, pp. 2169–84.
34. I. Tuah-Poku, M. Dollar, and T.H.B. Massalski: *Metall. Trans. A*, 1988, vol. 19A, pp. 675–86.
35. J. Crank: *The Mathematics of Diffusion*, Oxford University Press, Oxford, 1979.
36. M.-C. Liu, G.-M. Sheng, H.-J. He, and Y.-J. Jiao: *J. Mater. Process. Technol.*, 2017, vol. 246, pp. 245–51.
37. A.T. Egbewande, C. Chukwukaeme, and O.A. Ojo: *Mater. Charact.*, 2008, vol. 59, pp. 1051–58.
38. E.D. Moreau and S.F. Corbin: *Metall. Mater. Trans. A*, 2019, vol. 50A, pp. 5678–88.
39. J.-O. Andersson, T. Helander, L. Höglund, P. Shi, and B.O. Sundman: *Calphad*, 2002, vol. 26, pp. 273–12.
40. A. Schnell, A. Stankowski and E. de Marcos: *A study of the diffusion brazing process applied to the single crystal superalloy CMSX-4*. (2006).
41. J. Ruiz-Vargas, N. Siredey-Schwaller, N. Gey, P. Bocher, and A. Hazotte: *J. Mater. Process. Technol.*, 2013, vol. 213, pp. 20–29.
42. T. Tokunaga, K. Nishio, and M. Hasebe: *J. Phase Equilib.*, 2001, vol. 22, pp. 291–99.
43. Thermo-Calc Software TCNI /NI-alloys database version 10, ((accessed 06 August 2021)).
44. W.D. MacDonald and T.W. Eagar: *Metall. Mater. Trans. A*, 1998, vol. 29A, pp. 315–25.
45. D.A. Porter and K.E. Easterling: *Phase Transformations in Metals and Alloys (Revised Reprint)*, CRC Press, Boca Raton, 2009.
46. H. Kokawa, C.H. Lee, and T.H. North: *Metall. Trans. A*, 1991, vol. 22A, pp. 1627–31.
47. W.F. Gale and E.R. Wallach: *Metall. Trans. A*, 1991, vol. 22A, pp. 2451–57.
48. M. Pouranvari, A. Ekrami, and A.H. Kokabi: *Sci. Technol. Weld. Joining*, 2018, vol. 23, pp. 13–18.
49. A. LeBlanc and R. Mevrel, In *Conference proceedings: High Temperature Materials for Power Engineering*, (Liege Belgium: 1990), pp 1451–60.
50. B. Zhang, G. Sheng, Y. Jiao, Z. Gao, X. Gong, H. Fan, and J. Zhong: *J. Alloy. Compd.*, 2017, vol. 695, pp. 3202–10.
51. S. Steuer and R.F. Singer: *Metall. Mater. Trans. A*, 2013, vol. 44A, pp. 2226–32.
52. N. Sheng, J. Liu, T. Jin, X. Sun, and H. Zhuangqi: *J. Mater. Sci. Technol.*, 2015, vol. 31, pp. 129–34.
53. N. Sheng, J. Liu, T. Jin, X. Sun, and H. Zhuangqi: *Metall. Mater. Trans. A*, 2015, vol. 46, pp. 5772–81.
54. S.F. Corbin and C.A. Tadgell: *Metall. Mater. Trans. A*, 2021, vol. 52A, pp. 1232–47.
55. E.D. Moreau and S.F. Corbin: *Metall. Mater. Trans. A*, 2020, vol. 51A, pp. 3906–19.
56. C. Tadgell and S.F. Corbin: *Can. Metall. Q.*, 2020, vol. 59, pp. 288–96.
57. S. Steuer and R.F. Singer: *Metall. Mater. Trans. A*, 2014, vol. 45A, pp. 3545–53.
58. M. Pouranvari, A. Ekrami, and A.H. Kokabi: *J. Alloy. Compd.*, 2009, vol. 469, pp. 270–75.
59. C.W. Sinclair: *J. Phase Equilib.*, 1999, vol. 20, pp. 361–69.